ACS NANO
Cite This: ACS Nano 2018, 12, 12713–12720
www.acsnano.org

ARTICLE

Quasi-1D TiS_3 Nanoribbons: Mechanical Exfoliation and Thickness-Dependent Raman Spectroscopy

Alexey Lipatov,[†] Michael J. Loes,[†] Haidong Lu,[‡] Jun Dai,[†] Piotr Patoka,[§] Nataliia S. Vorobeva,[†] Dmitry S. Muratov,[†,∥] Georg Ulrich,[§,⊥] Bernd Kästner,[⊥] Arne Hoehl,[⊥] Gerhard Ulm,[⊥] Xiao Cheng Zeng,[†,#] Eckart Rühl,[§] Alexei Gruverman,[‡,#] Peter A. Dowben,[‡,#] and Alexander Sinitskii*[,†,#]

[†]Department of Chemistry, University of Nebraska, Lincoln, Nebraska 68588, United States
[‡]Department of Physics and Astronomy, University of Nebraska, Lincoln, Nebraska 68588, United States
[§]Physical Chemistry, Institut für Chemie und Biochemie, Freie Universität Berlin, 14195 Berlin, Germany
[∥]National University of Science and Technology "MISIS", Moscow 119991, Russia
[⊥]Physikalisch-Technische Bundesanstalt (PTB), Abbestraße 2-12, 10587 Berlin, Germany
[#]Nebraska Center for Materials and Nanoscience, University of Nebraska, Lincoln, Nebraska 68588, United States

Supporting Information

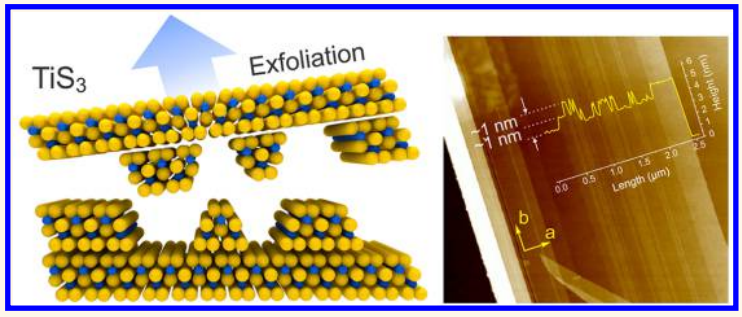

ABSTRACT: Quasi-one-dimensional (quasi-1D) materials enjoy growing interest due to their unusual physical properties and promise for miniature electronic devices. However, the mechanical exfoliation of quasi-1D materials into thin flakes and nanoribbons received considerably less attention from researchers than the exfoliation of conventional layered crystals. In this study, we investigated the micromechanical exfoliation of representative quasi-1D crystals, TiS_3 whiskers, and demonstrate that they typically split into narrow nanoribbons with very smooth, straight edges and clear signatures of 1D TiS_3 chains. Theoretical calculations show that the energies required for breaking weak interactions between the two-dimensional (2D) layers and between 1D chains within the layers are comparable and, in turn, are considerably lower than those required for breaking the covalent bonds within the chains. We also emulated macroscopic exfoliation experiments on the nanoscale by applying a local shear force to TiS_3 crystals in different crystallographic directions using a tip of an atomic force microscopy (AFM) probe. In the AFM experiments, it was possible to slide the 2D TiS_3 layers relative to each other as well as to remove selected 1D chains from the layers. We systematically studied the exfoliated TiS_3 crystals by Raman spectroscopy and identified the Raman peaks whose spectral positions were most dependent on the crystals' thickness. These results could be used to distinguish between TiS_3 crystals with thickness ranging from one to about seven monolayers. The conclusions established in this study for the exfoliated TiS_3 crystals can be extended to a variety of transition metal trichalcogenide materials as well as other quasi-1D crystals. The possibility of exfoliation of TiS_3 into narrow (few-nm wide) crystals with smooth edges could be important for the future realization of miniature device channels with reduced edge scattering of charge carriers.

KEYWORDS: *quasi-one-dimensional materials, transition metal trichalcogenides, Raman spectroscopy, mechanical exfoliation, scanning near-field optical microscopy*

Mechanical exfoliation of layered materials using the simple adhesive tape approach is an important technique for producing high-quality two-dimensional (2D) crystals for research at the interface of materials

Received: October 9, 2018
Accepted: November 20, 2018
Published: November 30, 2018

DOI: 10.1021/acsnano.8b07703
ACS Nano 2018, 12, 12713–12720

science and condensed matter physics.[1] The layered materials, such as graphite, a large family of transition metal dichalcogenides, hexagonal boron nitride (h-BN), and many others, are very diverse in terms of their chemical composition and physical properties.[2−4] But what they have in common is that they consist of charge-neutral 2D sheets with strong covalent or ionic bonding between the atoms within the sheets (in two dimensions) and weak interaction between the sheets (in the third dimension).

A different class of solids that shares many similarities with these layered crystals but received considerably less attention are quasi-one-dimensional (quasi-1D) materials.[5−8] Titanium trisulfide (TiS_3) is a representative quasi-1D material. It is an n-type semiconductor with a band gap of about 1 eV.[8−11] It was studied for several decades with regard to its prospects for energy storage applications,[12−14] but recently received a surge of attention due to the theoretical predictions of high electron mobilities[15,16] and promising thermoelectric properties.[14,17,18] The crystal structure of TiS_3 is shown in Figure 1a.[5] Similar to the layered crystals, quasi-1D materials are built through interplay of strong covalent bonds and weak van der Waals-like interactions. However, in TiS_3 and other transition metal trichalcogenide (TMTC) crystals with MX_3 composition (M is a transition metal ion, such as Ti, Zr, or Hf; X = S, Se, or Te), a basic covalently bound structural unit is not a layer but a 1D chain of MX_3 prisms (Figure 1a).[6−8] The weak van der Waals-

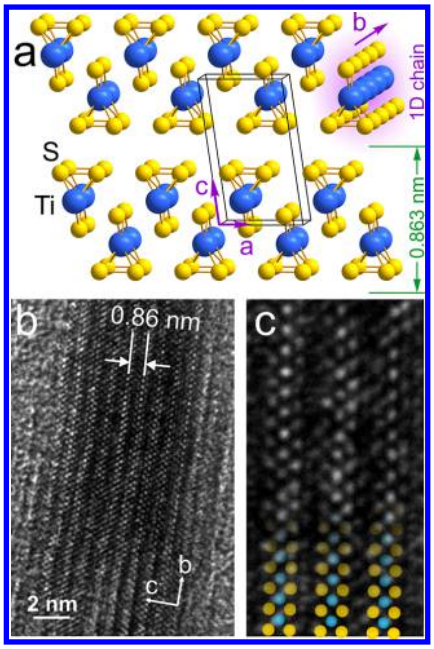

Figure 1. One-dimensional chains in TiS_3 structure. (a) Scheme of the monoclinic TiS_3 crystal structure with a $P2_1/m$ space group and the interlayer distance of 0.863 nm. (b, c) High-resolution TEM images of a TiS_3 crystal. In (c), the TiS_3 chains are overlaid with blue and yellow circles representing Ti and S atoms, respectively.

like interactions assemble these chains into 2D layers, and then the layers stack into 3D crystals. The 1D chains of TiS_3 crystals can be visualized by transmission electron microscopy (TEM) (Figure 1b,c). They consist of trigonal prisms formed by sulfide (S^{2-}) and disulfide (S_2^{2-}) units with Ti^{4+} in the center. TEM image showing the chains perpendicular to the *ab* plane is presented in Figure S4 together with the corresponding selected area electron diffraction (SAED) pattern.

TiS_3 crystals were prepared through a direct reaction between metallic titanium and sulfur vapor at 550 °C (Figure S1)[19,20] and characterized by spectroscopic techniques (Figure S2 and Figure S3). Because of their anisotropic structure, TiS_3 crystals usually grow in a form of whiskers (Figure 2a and Figure S5) with their long axis corresponding to the crystallographic *b* direction of 1D chains (Figure 1a). Like graphite or similar layered crystals,[1] these TiS_3 whiskers could be placed on an adhesive tape and subjected to micromechanical exfoliation, which was done in a number studies aiming to investigate thin TiS_3 flakes.[21−26] However, while the micromechanical exfoliation is well-established for the layered crystals, it received much less attention for quasi-1D crystals. For TiS_3 and similar crystals, this process is rather peculiar since weak interactions are present in two crystallographic directions, *a* and *c*, and when a mechanical

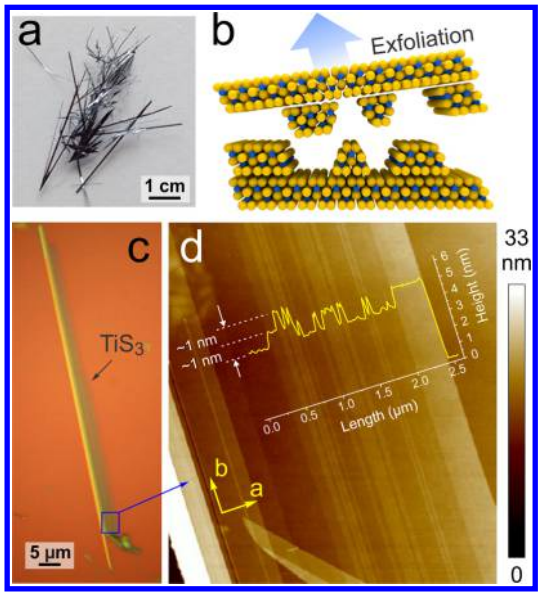

Figure 2. Visualization of one-dimensional chains in TiS_3 whiskers. (a) Optical photograph of TiS_3 whiskers. (b) Scheme of micromechanical exfoliation of TiS_3. (c) Optical image of an exfoliated TiS_3 nanoribbon on Si/SiO_2. (d) AFM image of a small area of the TiS_3 nanoribbon shown in (c). Overlaid over the image is the height profile across the nanoribbon.

force is applied to a crystal, it could split into thinner flakes along both directions.

In this work, we demonstrate that micromechanical exfoliation of quasi-1D crystals (Figure 2b,c,d) can produce thin flakes with morphologies very different from those typically observed for the layered crystals with weak interlayer bonding. It was previously reported that because of their quasi-1D structure, the TiS_3 crystals typically split into narrow nanoribbons with very smooth and straight edges rather than randomly shaped flakes.[22] We further demonstrate that the surfaces of the exfoliated flakes are not necessarily atomically smooth but could bear signatures of the 1D TiS_3 chains. These observations are supported by the theoretical analysis of the cleavage energies for various crystallographic planes in the TiS_3 structure. The calculations show that breaking weak bonding interactions between the 2D layers and between 1D chains within the layers require comparable energies, which in turn are considerably lower than those required for breaking the covalent bonds within the chains. We also emulated macroscopic exfoliation experiments on the nanoscale by applying a local shear force to TiS_3

DOI: 10.1021/acsnano.8b07703
ACS Nano 2018, 12, 12713−12720

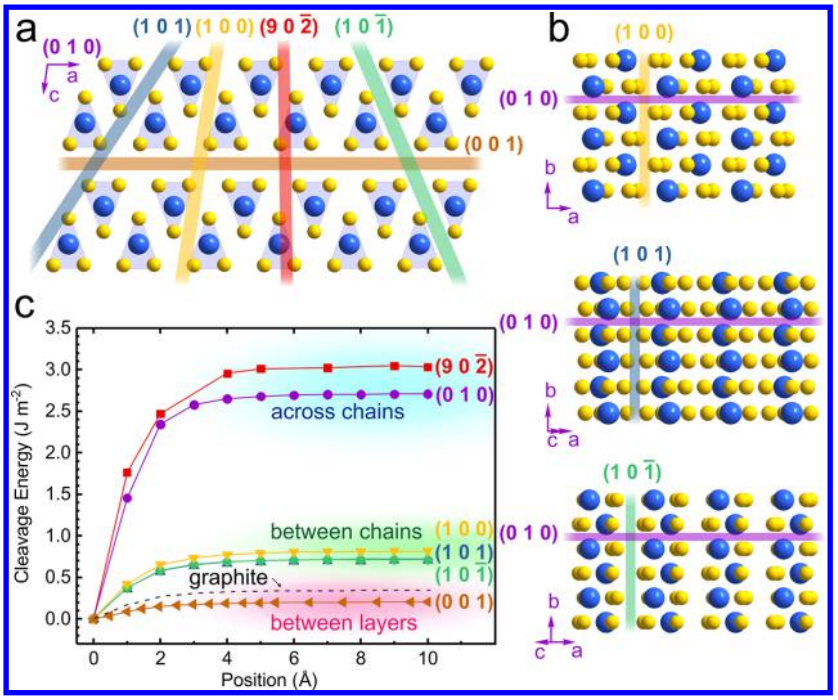

Figure 3. Cleavage energy calculations for different crystallographic planes in TiS_3. (a) Scheme of the planes in the TiS_3 structure that were considered for cleavage energy calculations. The plane of the image is (010). (b) Additional views of the TiS_3 structure along the selected crystallographic directions showing that the (100), (101), and (10$\bar{1}$) planes separate TiS_3 chains and do not dissect any of the covalent Ti−S bonds. (c) Cleavage energies for various scenarios from (a) and (b) plotted as a function of the separation between the planes.

crystals in different crystallographic directions using a tip of an atomic force microscopy (AFM) probe. In the AFM experiments, it was possible to slide the weakly interacting TiS_3 layers relative to each other as well as to detach the selected 1D chains from the layers. Raman spectroscopy revealed a considerable shift of the wavenumbers of the two modes in opposite directions with the number of layers, which provides a facile way to determine thicknesses of exfoliated TiS_3 flakes. Finally, we used infrared (IR) scattering-type near-field optical microscopy (s-SNOM) to correlate an IR response with an AFM image of an exfoliated TiS_3 crystal on Si/SiO_2 and observed the strong light scattering ability of the edges of TiS_3 terraces with well-defined topographic steps, which is directly related to the uniformity of the quasi-1D TiS_3 chains observed by AFM and TEM. The conclusions established in this study for the exfoliated TiS_3 crystals can likely be extended to other TMTC materials as well as other quasi-1D crystals.

RESULTS AND DISCUSSION

The peculiarity of the micromechanical exfoliation of TiS_3 crystals can be illustrated by the AFM image in Figure 2d. Unlike exfoliated flakes of graphene, h-BN, and other 2D materials, which are typically very flat, the TiS_3 crystals often show a structure of parallel stripes that run along the entire length of a crystal. These stripes have very uniform heights and widths. The height profile measured across these stripes shows that they exhibit the same step height of about 1 nm, which corresponds to the thickness of a 2D layer in the TiS_3 structure (Figure 1a). Thus, these stripes represent the residual 1D chains of two topmost layers of the exfoliated TiS_3 crystal. The observed uniformity of these stripes suggests that the splitting of these layers likely happened in between the weakly bound chains, as shown in Figure 2b.

In order to support this conclusion, we investigated cleavage energies for different crystallographic planes in the TiS_3 structure. Since the stripes were observed along the crystallographic *b* direction (Figure 2d), we considered several cleavage planes that were parallel to it; see Figure 3a. Some of these planes, such as (100), (101), and (10$\bar{1}$), propagate between the TiS_3 chains, while (90$\bar{2}$), which is nearly perpendicular to the (001) planes, dissects the TiS_3 chains. This is further illustrated by Figure 3b, which demonstrates additional views of the TiS_3 crystal structure orthogonal to (100), (101), and (10$\bar{1}$) planes; the figure shows that these planes separate TiS_3 chains and do not dissect any of the covalent Ti−S bonds. For the sake of comparison, we also considered the (010) plane, which is perpendicular to the crystallographic *b* direction and cuts the TiS_3 chains.

The results of the cleavage energy calculations for these crystallographic planes are shown in Figure 3c. The lowest cleavage energy was found for the (001) planes, which separate the 2D TiS_3 layers. As shown in Figure 3c, the energy increases with the separation between the layers and converges to 0.204 J m^{-2}. As noted in the previous report,[15] this energy is lower than the cleavage energy for graphene layers in graphite crystal, which is shown by the dashed line in Figure 3c and converges at about 0.320 J m^{-2}. This computational result suggests that the exfoliation of 2D layers of TiS_3 crystals should be even easier than the exfoliation of graphene from graphite. Figure 3c also shows that other planes that separate the TiS_3 chains without dissecting the covalent Ti−S bonds have comparable cleavage energies converging at 0.714, 0.716, and 0.815 J m^{-2} for the (101), (10$\bar{1}$), and (100) planes, respectively. These values are only about twice as large as the cleavage energies of graphite, suggesting that the mechanical exfoliation separating TiS_3 chains without breaking them is highly feasible. On the contrary, the planes that dissect the covalent bonds within the TiS_3 chains

DOI: 10.1021/acsnano.8b07703
ACS Nano 2018, 12, 12713−12720

were found to have much higher cleavage energies, such as 2.706 J m^{-2} for the (010) planes and 3.03 J m^{-2} for the $(90\bar{2})$ planes (Figure 3c). Overall, the calculations show that comparable energies are required for breaking the weak interactions between the 2D layers and between 1D chains within the layers. Furthermore, these energies are considerably lower than those required for breaking the covalent bonds within the chains. These computational results agree well with the experimentally observed exfoliation of TiS_3, as the ease of cleavage between the 1D chains is consistent with the stripy pattern in the AFM image (Figure 2d). Also, the stripes have uniform widths, because as the cleavage starts in the crystallographic *b* direction between the chains, it is unlikely to deviate in the *a* direction since breaking covalent bonds within the chains requires higher energy. The ease of cleavage between the 1D chains is also consistent with the very smooth and straight edges of the exfoliated TiS_3 nanoribbons.

While the mechanical exfoliation of layered materials is usually performed on the macroscale by the manual peeling of crystals using an adhesive tape, it can also be realized on the nanoscale using an AFM tip. Figure 4a shows the scheme of the experiment, in which a diamond-coated tip is pressed against a TiS_3 crystal with a force of 2−10 μN and then dragged either along or across the direction of 1D chains. The purpose of this experiment was to verify the results of theoretical simulations (Figure 3), which predicted that the interactions between the 2D layers and between the 1D chains within the layers are rather weak compared to the covalent bonding within the chains. The advantage of the described AFM experiment is that these interactions could be probed separately by first dragging an AFM tip along the chains to study how they exfoliate from other chains within the 2D layers, and then dragging it across the chains to see how the weakly interacting 2D layers slide relative to each other.

Figure 4b shows an AFM image of a TiS_3 crystal, which was scratched with a force of ~10 μN in the direction marked by the red arrow. The moving tip cleaved the 1D chains from the underlying 2D layer and the surrounding chains within the layer, forming a well-visible scratch. The chains are pushed forward and accumulated together in a structure indicated by the blue arrow in Figure 4b. This cleavage scenario is illustrated by Figure 4a, in which the tip does not move across the covalently bonded 1D chains that require relatively high energies for breaking (Figure 3).

The situation changes when the AFM tip scratches an exfoliated TiS_3 crystal along the *a* direction. Since diamond is much harder than TiS_3, it can also cut the 1D chains across if a sufficient force is applied to the tip, which we observed experimentally in some cases. However, Figure 4c−e shows another possible scenario, in which the tip moving across a TiS_3 nanoribbon slides the top 2D layers relative to the bottom layers, again providing evidence for the weak interlayer interactions. Figure 4c shows an AFM image of a fragment of as-prepared TiS_3 crystal. Figure 4d shows that the first drag of an AFM tip across this crystal with a force of ~2 μN causes the top 2D layers to slide to the side, while the second drag along the same trajectory with a force of ~3 μN cleaves more 2D layers in a similar manner (Figure 4e). Overall, the nanoscale cleavage experiments further demonstrate the ease with which TiS_3 crystals can be exfoliated along the weakly bound 2D layers as well as 1D chains.

In the framework of this study, we exfoliated a large number of TiS_3 crystals with different thicknesses, which could be assessed

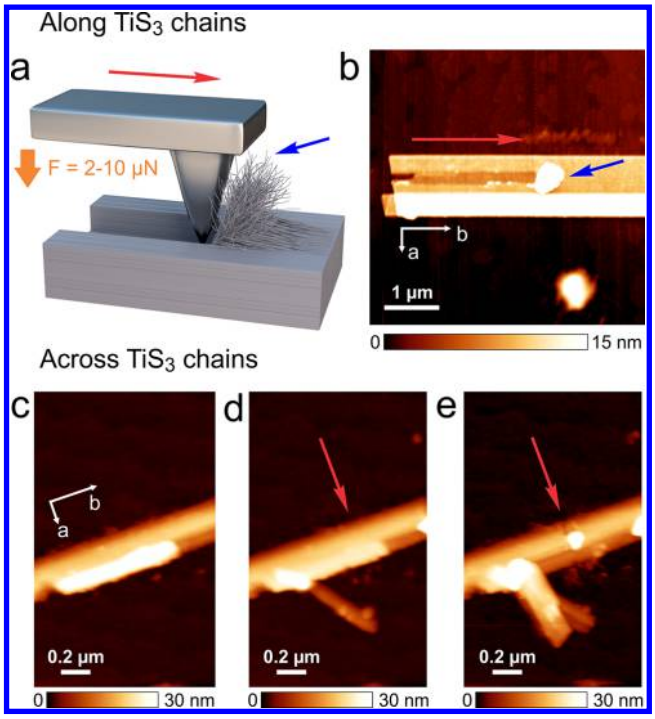

Figure 4. Nanomechanical exfoliation of TiS_3 crystals using an AFM tip. (a) Scheme of the experiment. (b) AFM image of a TiS_3 crystal on a barium titanite ($BaTiO_3$) substrate that was cleaved by an AFM tip *along* the 1D chains. Tip force: ~10 μN. (c−e) AFM images of a TiS_3 crystal on a $BaTiO_3$ substrate that was cleaved *across* the 1D chains: (c) as-prepared crystal, (d) the same crystal after the first cleavage (tip force: ~2 μN), and (e) the same crystal after the second cleavage (tip force: ~3 μN). The red arrows show the AFM tip cleavage direction.

by Raman spectroscopy. Several recent studies focused on understanding the origin and behavior of the Raman-active modes in TiS_3 and related TMTCs.[27−30] However, there is still a lack of information regarding the most common practical application of Raman spectroscopy to 2D materials, which is the determination of the number of monolayers in thin crystals. For example, Raman spectroscopy was shown to be a powerful tool for determining the number of monolayers in the most studied 2D materials, such as graphene,[31] hexagonal boron nitride,[32] MoS_2,[33,34] and WS_2,[35] but information on how to distinguish between monolayer and few-layer TiS_3 crystals is still missing in the literature.

There are several experimental complications for the Raman spectroscopy investigation of TiS_3 crystals with different thicknesses. First of all, since many exfoliated TiS_3 crystals have terraced surfaces, as shown in Figure 2d and Figure S6, they cannot be assigned to a specific number of layers. Second, since the splitting between the TiS_3 chains is nearly as easy as the splitting between the TiS_3 layers, during the exfoliation process the crystals typically get not only thinner but also narrower and often become too narrow for Raman spectroscopy. A monolayer (1L) TiS_3 nanoribbon that is only a few nanometers wide can be seen in Figure 5a. The observation of such narrow ribbons is interesting in the view of their potential application in nanoscale electronic devices, but characterization of such narrow TiS_3 crystals by conventional Raman microscopy with a focused laser beam spot of about 2 μm is problematic. In this study, we were able to identify a sufficient number of TiS_3 nanoribbons that had smooth surfaces and were wide enough for Raman spectroscopy.

DOI: 10.1021/acsnano.8b07703
ACS Nano 2018, 12, 12713−12720

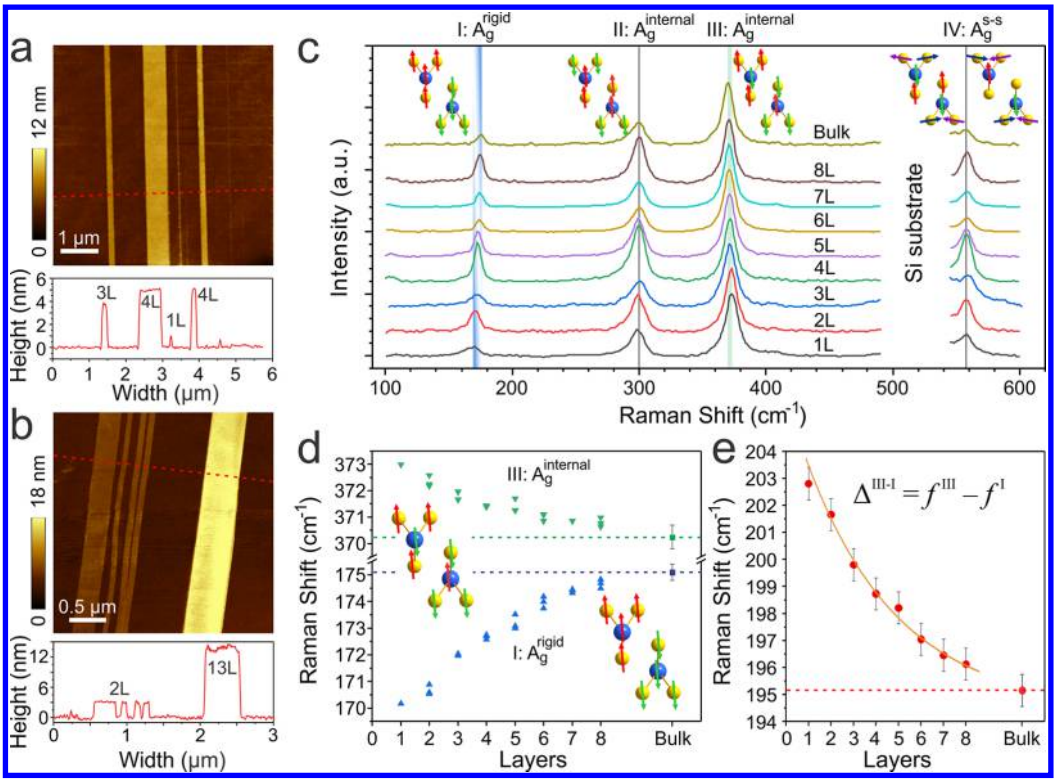

Figure 5. Thickness-dependent Raman spectroscopy of TiS_3 flakes. (a, b) AFM images of TiS_3 nanoribbons with different thicknesses and the corresponding height profiles. (c) Raman spectra of exfoliated TiS_3 flakes with different thicknesses. Raman-active modes are named according to ref 27 and are shown above the corresponding Raman peaks. (d) Wavenumbers f^I (blue ▲) and f^{III} (green ▼) of $I:A_g^{rigid}$ and $III:A_g^{internal}$ Raman-active modes, respectively, plotted as a function of the number of layers in exfoliated TiS_3 crystals. Data points show wavenumbers from individual experiments. The peak positions for bulk TiS_3 were averaged over 25 samples and are shown with error bars. (e) Averaged difference $\Delta^{III-I} = f^{III} - f^I$ of the wavenumbers of $III:A_g^{internal}$ and $I:A_g^{rigid}$ Raman-active modes in TiS_3 as a function of the number of layers. The error bars indicate the standard deviation of uncertainty based on the statistical analysis of Raman measurements of 25 bulk TiS_3 samples.

Examples of TiS_3 crystals with thicknesses up to 13 layers (13L) are shown in Figure 5a,b. The numbers of layers in these and similar images were assigned based on the entire set of AFM data. In the AFM images, monolayers of layered 2D materials often exhibit larger thicknesses in comparison with the expected theoretical thicknesses, which is attributed to the presence of water adsorbates and other contaminants.[1,36] In our AFM experiments, monolayer TiS_3 crystals were about 2 nm thick, and the thickness of thicker TiS_3 crystals increased by ~0.9 nm per every additional layer.

Typical Raman spectra of TiS_3 flakes are shown in Figure 5c. The range from 490 to 530 cm^{-1} is not shown, as it includes spectroscopic response from the Si/SiO_2 substrate. We did not observe any Raman peaks related to TiS_3 at wavenumbers higher than 600 cm^{-1}, as shown in Figure S7. In the 100−600 cm^{-1} range, we observed four A_g Raman-active modes at f^I = 175 cm^{-1}, f^{II} = 300 cm^{-1}, f^{III} = 370 cm^{-1}, and f^{IV} = 560 cm^{-1}, which correspond to $I:A_g^{rigid}$, $II:A_g^{internal}$, $III:A_g^{internal}$, and $IV:A_g^{S-S}$, respectively; the peaks were assigned based on the calculations by Wu *et al.*[27] The positions of two of the four observed peaks, f^{II} and f^{IV}, did not exhibit significant dependences on the number of layers. In the $II:A_g^{internal}$ mode the vibrations occur out-of-plane, but both trigonal prismatic chains are moving collectively in the same direction, making intralayer interactions dominant. The $IV:A_g^{S-S}$ corresponds to in-plane vibrations of the S_2^{2-} groups in the same trigonal prismatic chain, so interlayer interactions do not significantly affect the wavenumber of this mode. However, we found a considerable downshift of the f^I wavenumber of the $I:A_g^{rigid}$ mode from 175 cm^{-1} to 170 cm^{-1} on decreasing the number of layers. There was also a noticeable increase of the f^{III} wavenumber of the $III:A_g^{internal}$ mode from 370 cm^{-1} to 373 cm^{-1} with the decrease of the number of layers (Figure 5d). These two modes have two trigonal prismatic chains moving in the opposite directions showing dominance of the interchain interaction, which reflects the quasi-1D structure of TiS_3, similar to ZrS_3 and $ZrSe_3$.[28] Since the f^I and f^{III} wavenumbers shift in the opposite directions with increasing thickness of TiS_3, it is convenient to use their difference $\Delta^{III-I} = f^{III} - f^I$ to distinguish the number of layers in thin TiS_3 crystals (Figure 5e). A similar approach was successfully used for monolayer and few-layer MoS_2 flakes.[33,34] The Δ^{III-I} peak difference varies in a wider range (from 195 to 203 cm^{-1}) than any of the individual peaks, and while the positions of the individual peaks should be carefully measured *versus* a calibrated standard, the use of their difference eliminates systematic measurement errors.

Finally, we investigated exfoliated TiS_3 crystals on a Si/SiO_2 substrate by the IR scattering-type scanning near-field optical microscopy using an s-SNOM system that is schematically shown in Figure 6a. The system includes an atomic force microscope operated in the tapping mode and an asymmetric Michelson interferometer. Incident IR radiation of a CO_2 gas laser is scattered on a Au-coated silicon AFM cantilever, which has a resonance frequency of about 130 kHz. In this experiment, simultaneously to the topography, we measured the IR response from the broad SiO_2 substrate phonon (ranging from 900 to 1250 cm^{-1}) through the exfoliated TiS_3 crystal shown in the AFM image in Figure 6b. The near-field intensity maps were

DOI: 10.1021/acsnano.8b07703
ACS Nano 2018, 12, 12713−12720

collected at 1080 cm^{-1}, the lowest wavenumber that is still accessible by the CO_2 laser. By tuning to off-resonance we

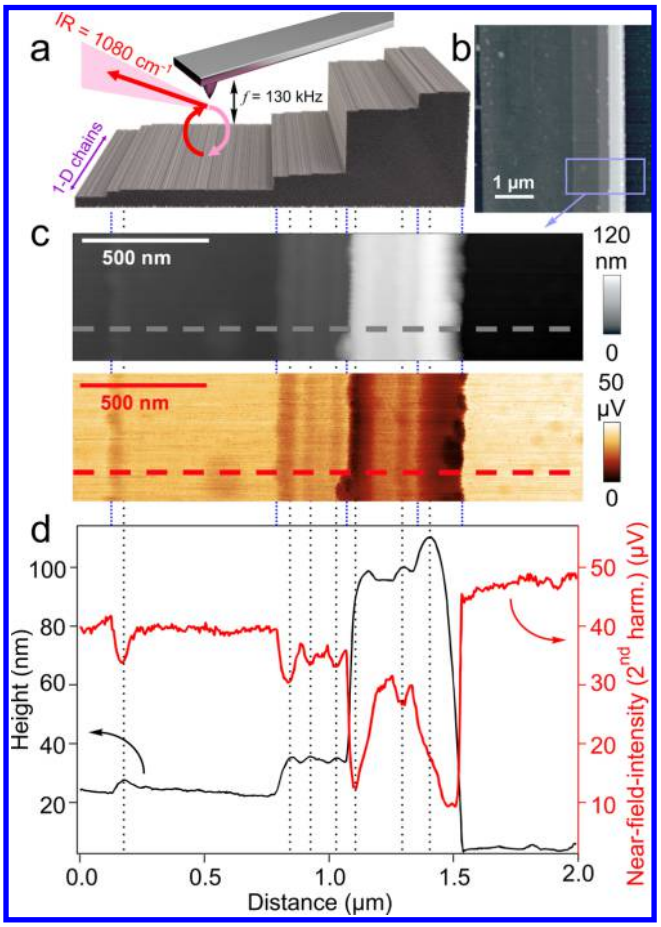

Figure 6. Scanning near-field optical microscopy of exfoliated TiS_3 flakes. (a) Scheme of the operation principle of the s-SNOM with incident laser light scattered at the tip's apex, locally exciting the sample. The tip is oscillating at 130 kHz and collecting the chemical contrast simultaneously with the topography, while scanning the sample's surface. (b) Topography map from an AFM scan over an exfoliated TiS_3 crystal on Si/SiO_2. (c) High-resolution scan from the blue-marked area in (b), showing the topography of the step-like structure (top) of the TiS_3 surface and the near-field-intensity map (bottom) collected using the laser radiation operating at 9.261 μm (1080 cm^{-1}) at the second harmonic of the tip's oscillation frequency. (d) Cross section lines representing the topography (black) and the near-field intensity (red) across the TiS_3 steps shown in (c). Step edges (dashed blue lines) and other topographic and IR absorption features (dashed black lines) are indicated.

avoided artifacts from the peak shifts due to the sample–substrate interactions, as reported in the previous near-field spectroscopic studies in the mid-infrared regime.[37,38] The spectroscopic response did not include a signal from the TiS_3 crystal, which shows infrared features at much lower wavenumbers in the spectral range that is not accessible to the used light source and is below the detector's sensitivity range.

Figure 6c shows a high-resolution 2 μm × 0.25 μm scan of the marked blue area of the exfoliated TiS_3 crystal shown in Figure 6b. The upper part of Figure 6c is a topographic representation of the TiS_3 whisker, while the bottom part is a near-field intensity map collected at the second harmonic of the tip oscillation frequency. For a clearer view, in Figure 6d we overlay the AFM cross section of the sample (black line), which was measured along the dashed gray line in Figure 6c, and the simultaneously acquired near-field signal (red line), which corresponds to the dashed red line in Figure 6c. Figure 6d shows that the near-field intensity drops at the positions of the edges of the TiS_3 whisker terraces. The intensity attenuation is not constant along the entire TiS_3 step structure and slightly recovers toward the next terrace and drops again in the presence of another edge. Additionally, the near-field signal intensity drop is deeper depending on the height difference between the involved terraces. As mentioned above, the near-field signal at 1080 cm^{-1} is characteristic for the underlying SiO_2 substrate and is due to the strong optical response from the SiO_2 phonon resonance peaking at 1130 cm^{-1}. The intensity of the near-field response originating from the SiO_2 phonon is strongly dependent on the tip–sample interactions. The presence of TiS_3 on top of SiO_2 is directly affecting the coupling of the infrared radiation focused by the tip to the SiO_2 phonon, which results in near-field intensity drops, leading to strong discontinuities at the terrace edges. However, in the optical intensity signal, these strong discontinuities are not restricted just to edges, but propagate well into terraces, suggesting that this effect is strongest at the terrace edge, but also affects the terraces. Considering the TiS_3 crystal structure and the appearance of the exfoliated nanoribbons in Figure 2d, the suppression of the substrate phonon responses near the edges of crystal terraces in the s-SNOM measurements are consistent with the structure of the quasi-1D TiS_3 chains, which form terraces with well-defined topographic steps, demonstrating strong light-scattering ability.

CONCLUSIONS

In summary, TiS_3 nanoribbons with straight and smooth edges showing clear signatures of 1D chains were produced by micromechanical exfoliation. The observed structures form due to the drastically different cleavage energies for various crystallographic planes. The theoretical calculations show that breaking weak interactions between the 2D layers and between 1D chains within the layers requires comparable energies, which in turn are considerably higher than those required for breaking the covalent bonds within the chains. The macroscopic exfoliation experiments were emulated on the nanoscale by applying a local shear force to TiS_3 crystals along different crystallographic directions using an AFM tip. In the AFM experiments it was possible to both slide the 2D TiS_3 layers relative to each other and remove selected 1D chains from the layers. We systematically studied the exfoliated TiS_3 crystals by Raman spectroscopy and demonstrated which Raman peaks are most dependent on the crystals' thickness. These results could be used to distinguish between TiS_3 crystals with thicknesses ranging from one to about seven monolayers. Finally, by using the s-SNOM technique we correlated an IR response with a topographic image of an exfoliated TiS_3 crystal on a Si/SiO_2 substrate and observed strong light scattering at the edges of TiS_3 terraces with well-defined topographic steps, which is directly related to the uniformity of the quasi-1D TiS_3 chains observed by AFM and TEM. The conclusions established in this study for the exfoliated TiS_3 crystals can likely be extended to other TMTC materials as well as other quasi-1D crystals. The possibility of exfoliation of TiS_3 into crystals with smooth edges could be important for the future realization of miniature 2D device channels with reduced edge scattering of charge carriers.

DOI: 10.1021/acsnano.8b07703
ACS Nano 2018, 12, 12713–12720

METHODS

Cleavage Energy Calculations. The cleavage energy calculations were carried out using density functional theory (DFT) methods within the generalized gradient approximation (GGA) and with the Perdew–Burke–Ernzerhof (PBE) exchange–correlation functional, as implemented in the Vienna *ab initio* simulation package (VASP).[39] The Grimme's D3 dispersion correction was adopted to account for the long-range interactions. The ion–electron interaction was treated using the projector-augmented-wave (PAW) technique, and a kinetic energy cutoff of 500 eV was chosen. The cleavage was simulated by introducing a fracture in the TiS_3 ribbon where the edges were passivated with hydrogen. The total energies under variation of the separation between the fractured parts were computed to simulate the cleavage process. The representative cleavage energy calculation for the (101) planes is illustrated by Figure S8.

Transmission Electron Microscopy. The microstructure of TiS_3 flakes was studied using a FEI Tecnai Osiris scanning transmission electron microscope equipped with a HAADF detector and an X-FEG high-brightness Schottky field emission gun. The accelerating voltage was 200 kV. For the sample preparation we used TiS_3 crystals, which were collected from the surface of a quartz ampule (Figure S1) and sonicated in dehydrated ethanol for 1 min. The suspension was drop cast on a TEM grid (Cu grid with lacey carbon; Ted Pella #01890), dried in air, and immediately loaded into the TEM instrument.

Exfoliation by AFM Tip. The nanoscale cleavage experiments were performed on a commercial AFM system (MFP3D, Asylum Research) using diamond-coated AFM tips (CDT-NCHR, Nanosensors) with a spring constant of about 40 N/m. To cleave the 1D chains, the tip was scanned either along or perpendicularly to the chain direction with a constant speed of 200 nm/s under a constant loading force in the range from 0.5 to 10 μN. The loading force magnitude had a profound effect on the cleavage process: there was no cleavage at low forces (<1 μN), partial cleavage of the top layers occurred at medium forces (2–3 μN) when scanning perpendicularly to the chains, while even higher forces (>5 μN) were required to cleave the top layers when the AFM tip was scanned along the TiS_3 chains.

Infrared Scattering-Type Near-Field Optical Microscopy. The experimental setup has been described in detail in previous studies.[38,40,41] It consists of a commercial s-SNOM system (NeaSNOM, Neaspec GmbH), which includes an atomic force microscope operated in the tapping mode and an asymmetric Michelson interferometer. Au-coated (~30 nm) silicon AFM cantilevers with resonance frequencies of around 130 kHz were used as a scattering element of the microscope. The average tip diameter of near-field probes was below 50 nm. As for the IR radiation sources, we used a grating tuned CO_2 gas laser (PL5, Edinburgh Instruments) operating in sealed-off mode. This source is characterized by high intensity and frequency stability within a limited spectral range, which can be regarded as a suitable tool for nanoimaging experiments at discrete wavelengths.

Raman Spectroscopy. Raman spectra were measured at room temperature with a Thermo Scientific DXR Raman microscope operated in normal incidence and backscattered configuration. We used a 532 nm excitation laser, and the laser power was kept at 0.1 mW to prevent thermal damage to the flakes. A Si band at 520 cm^{-1} was used as a wavenumber reference. The spectral resolution was 0.96 cm^{-1}. The laser was focused through a 100× objective with a laser spot size on a sample of about 2 μm.

ASSOCIATED CONTENT

Supporting Information

The Supporting Information is available free of charge on the ACS Publications website at DOI: 10.1021/acsnano.8b07703.

Photographs illustrating the TiS_3 synthesis; X-ray photoelectron spectroscopy analysis; energy-dispersive X-ray spectrum, additional TEM and SAED images; SEM images; additional AFM images; additional Raman spectrum and description of cleavage energy calculation (PDF)

AUTHOR INFORMATION

Corresponding Author

*E-mail: sinitskii@unl.edu.

ORCID

Jun Dai: 0000-0001-6599-8826
Bernd Kästner: 0000-0002-6575-6621
Xiao Cheng Zeng: 0000-0003-4672-8585
Eckart Rühl: 0000-0002-0451-8734
Alexei Gruverman: 0000-0003-0492-2750
Peter A. Dowben: 0000-0002-2198-4710
Alexander Sinitskii: 0000-0002-8688-3451

Notes

The authors declare no competing financial interest.

ACKNOWLEDGMENTS

This research was supported by the National Science Foundation, through grants NSF ECCS-1740136 and ECCS-1508541, the nCORE, a wholly owned subsidiary of the Semiconductor Research Corporation (SRC), and the Nebraska Materials Research Science and Engineering Center (MRSEC) (NSF DMR-1420645). The materials characterization was performed in part in MISIS, in which the work was supported by the Ministry of Education and Science of the Russian Federation (K2-2018-014), and in the Nebraska Nanoscale Facility, which is supported by the NSF (ECCS-1542182) and the Nebraska Research Initiative. Financial support by the German Research Foundation (DFG) within SFB 1112 (TP B02) is also gratefully acknowledged.

REFERENCES

(1) Novoselov, K. S.; Jiang, D.; Schedin, F.; Booth, T. J.; Khotkevich, V. V.; Morozov, S. V.; Geim, A. K. Two-Dimensional Atomic Crystals. *Proc. Natl. Acad. Sci. U. S. A.* **2005**, *102*, 10451–10453.

(2) Geim, A. K.; Grigorieva, I. V. Van der Waals Heterostructures. *Nature* **2013**, *499*, 419–425.

(3) Butler, S. Z.; Hollen, S. M.; Cao, L.; Cui, Y.; Gupta, J. A.; Gutiérrez, H. R.; Heinz, T. F.; Hong, S. S.; Huang, J.; Ismach, A. F.; Johnston-Halperin, E.; Kuno, M.; Plashnitsa, V. V.; Robinson, R. D.; Ruoff, R. S.; Salahuddin, S.; Shan, J.; Shi, L.; Spencer, M. G.; Terrones, M.; et al. Progress, Challenges, and Opportunities in Two-Dimensional Materials Beyond Graphene. *ACS Nano* **2013**, *7*, 2898–2926.

(4) Bhimanapati, G. R.; Lin, Z.; Meunier, V.; Jung, Y.; Cha, J.; Das, S.; Xiao, D.; Son, Y.; Strano, M. S.; Cooper, V. R.; Liang, L.; Louie, S. G.; Ringe, E.; Zhou, W.; Kim, S. S.; Naik, R. R.; Sumpter, B. G.; Terrones, H.; Xia, F.; Wang, Y.; et al. Recent Advances in Two-Dimensional Materials Beyond Graphene. *ACS Nano* **2015**, *9*, 11509–11539.

(5) Furuseth, S.; Brattas, L.; Kjekshus, A. On the Crystal Structures of TiS_3, ZrS_3, $ZrSe_3$, $ZrTe_3$, HfS_3, and $HfSe_3$. *Acta Chem. Scand.* **1975**, *29*, 623–631.

(6) Srivastava, S. K.; Avasthi, B. N. Preparation, Structure and Properties of Transition Metal Trichalcogenides. *J. Mater. Sci.* **1992**, *27*, 3693–3705.

(7) Dai, J.; Li, M.; Zeng, X. C. Group IVB Transition Metal Trichalcogenides: A New Class of 2D Layered Materials Beyond Graphene. *Wiley Interdiscip. Rev.: Comput. Mol. Sci.* **2016**, *6*, 211–222.

(8) Island, J. O.; Molina-Mendoza, A. J.; Barawi, M.; Biele, R.; Flores, E.; Clamagirand, J. M.; Ares, J. R.; Sánchez, C.; van der Zant, H. S.; D'Agosta, R.; Ferrer, I. J.; Castellanos-Gomez, A. Electronics and Optoelectronics of Quasi-1D Layered Transition Metal Trichalcogenides. *2D Mater.* **2017**, *4*, No. 022003.

DOI: 10.1021/acsnano.8b07703
ACS Nano 2018, 12, 12713–12720

(9) Yi, H.; Komesu, T.; Gilbert, S.; Hao, G.; Yost, A. J.; Lipatov, A.; Sinitskii, A.; Avila, J.; Chen, C.; Asensio, M. C.; Dowben, P. A. The Band Structure of the Quasi-One-Dimensional Layered Semiconductor TiS_3(001). *Appl. Phys. Lett.* **2018**, *112*, No. 052102.
(10) Finkman, E.; Fisher, B. Electrical Transport Measurements in TiS_3. *Solid State Commun.* **1984**, *50*, 25−28.
(11) Ferrer, I. J.; Ares, J. R.; Clamagirand, J. M.; Barawi, M.; Sánchez, C. Optical Properties of Titanium Trisulphide (TiS_3) Thin Films. *Thin Solid Films* **2013**, *535*, 398−401.
(12) Murphy, D. W.; Trumbore, F. A. Chemistry of TiS_3 and $NbSe_3$ Cathodes. *J. Electrochem. Soc.* **1976**, *123*, 960−964.
(13) Zanini, M.; Shaw, J. L.; Tennenhouse, G. J. The Behavior of Na-TiS_2 and Na-TiS_3 as Solid-Solution Electrodes. *J. Electrochem. Soc.* **1981**, *128*, 1647−1650.
(14) Hayashi, A.; Matsuyama, T.; Sakuda, A.; Tatsumisago, M. Amorphous Titanium Sulfide Electrode for All-Solid-State Rechargeable Lithium Batteries with High Capacity. *Chem. Lett.* **2012**, *41*, 886−888.
(15) Dai, J.; Zeng, X. C. Titanium Trisulfide Monolayer: Theoretical Prediction of a New Direct-Gap Semiconductor with High and Anisotropic Carrier Mobility. *Angew. Chem., Int. Ed.* **2015**, *54*, 7572−7576.
(16) Kang, J.; Sahin, H.; Ozaydin, H. D.; Senger, R. T.; Peeters, F. M. TiS_3 Nanoribbons: Width-Independent Band Gap and Strain-Tunable Electronic Properties. *Phys. Rev. B: Condens. Matter Mater. Phys.* **2015**, *92*, No. 075413.
(17) Zhang, J.; Liu, X.; Wen, Y.; Shi, L.; Chen, R.; Liu, H.; Shan, B. Titanium Trisulfide Monolayer as a Potential Thermoelectric Material: A First-Principles-Based Boltzmann Transport Study. *ACS Appl. Mater. Interfaces* **2017**, *9*, 2509−2515.
(18) Morozova, N. V.; Korobeinikov, I. V.; Kurochka, K. V.; Titov, A. N.; Ovsyannikov, S. V. Thermoelectric Properties of Compressed Titanium and Zirconium Trichalcogenides. *J. Phys. Chem. C* **2018**, *122*, 14362−14372.
(19) Haraldsen, H.; Rost, E.; Kjekshus, A.; Steffens, A. On Properties of TiS_3, ZrS_3. *Acta Chem. Scand.* **1963**, *17*, 1283−1292.
(20) Brattas, L.; Kjekshus, A. On the Properties of Compounds with the $ZrSe_3$ Type Structure. *Acta Chem. Scand.* **1972**, *26*, 3441−3449.
(21) Island, J. O.; Buscema, M.; Barawi, M.; Clamagirand, J. M.; Ares, J. R.; Sánchez, C.; Ferrer, I. J.; Steele, G. A.; van der Zant, H. S. J.; Castellanos-Gomez, A. Ultrahigh Photoresponse of Few-Layer TiS_3 Nanoribbon Transistors. *Adv. Opt. Mater.* **2014**, *2*, 641−645.
(22) Lipatov, A.; Wilson, P. M.; Shekhirev, M.; Teeter, J. D.; Netusil, R.; Sinitskii, A. Few-Layered Titanium Trisulfide (TiS_3) Field-Effect Transistors. *Nanoscale* **2015**, *7*, 12291−12296.
(23) Island, J. O.; Barawi, M.; Biele, R.; Almazán, A.; Clamagirand, J. M.; Ares, J. R.; Sánchez, C.; van der Zant, H. S. J.; Álvarez, J. V.; D'Agosta, R.; Ferrer, I. J.; Castellanos-Gomez, A. TiS_3 Transistors with Tailored Morphology and Electrical Properties. *Adv. Mater.* **2015**, *27*, 2595−2601.
(24) Wang, M.; Li, C. M. Excitonic Properties of Graphene-Based Materials. *Nanoscale* **2012**, *4*, 1044−1050.
(25) Cui, Q.; Lipatov, A.; Wilt, J. S.; Bellus, M. Z.; Zeng, X. C.; Wu, J.; Sinitskii, A.; Zhao, H. Time-Resolved Measurements of Photocarrier Dynamics in TiS_3 Nanoribbons. *ACS Appl. Mater. Interfaces* **2016**, *8*, 18334−18338.
(26) Molina-Mendoza, A. J.; Island, J. O.; Paz, W. S.; Clamagirand, J. M.; Ares, J. R.; Flores, E.; Leardini, F.; Sánchez, C.; Agraït, N.; Rubio-Bollinger, G.; van der Zant, H. S. J.; Ferrer, I. J.; Palacios, J. J.; Castellanos-Gomez, A. High Current Density Electrical Breakdown of TiS_3 Nanoribbon-Based Field-Effect Transistors. *Adv. Funct. Mater.* **2017**, *27*, 1605647.
(27) Wu, K.; Torun, E.; Sahin, H.; Chen, B.; Fan, X.; Pant, A.; Parsons Wright, D.; Aoki, T.; Peeters, F. M.; Soignard, E.; Tongay, S. Unusual Lattice Vibration Characteristics in Whiskers of the Pseudo-One-Dimensional Titanium Trisulfide TiS_3. *Nat. Commun.* **2016**, *7*, 12952.
(28) Osada, K.; Bae, S.; Tanaka, M.; Raebiger, H.; Shudo, K.; Suzuki, T. Phonon Properties of Few-Layer Crystals of Quasi-One-Dimensional ZrS_3 and $ZrSe_3$. *J. Phys. Chem. C* **2016**, *120*, 4653−4659.
(29) Kong, W.; Bacaksiz, C.; Chen, B.; Wu, K.; Blei, M.; Fan, X.; Shen, Y.; Sahin, H.; Wright, D.; Narang, D. S.; Tongay, S. Angle Resolved Vibrational Properties of Anisotropic Transition Metal Trichalcogenide Nanosheets. *Nanoscale* **2017**, *9*, 4175−4182.
(30) Pawbake, A. S.; Island, J. O.; Flores, E.; Ares, J. R.; Sanchez, C.; Ferrer, I. J.; Jadkar, S. R.; van der Zant, H. S. J.; Castellanos-Gomez, A.; Late, D. J. Temperature-Dependent Raman Spectroscopy of Titanium Trisulfide (TiS_3) Nanoribbons and Nanosheets. *ACS Appl. Mater. Interfaces* **2015**, *7*, 24185−24190.
(31) Ferrari, A. C.; Meyer, J. C.; Scardaci, V.; Casiraghi, C.; Lazzeri, M.; Mauri, F.; Piscanec, S.; Jiang, D.; Novoselov, K. S.; Roth, S.; Geim, A. K. Raman Spectrum of Graphene and Graphene Layers. *Phys. Rev. Lett.* **2006**, *97*, 187401.
(32) Gorbachev, R. V.; Riaz, I.; Nair, R. R.; Jalil, R.; Britnell, L.; Belle, B. D.; Hill, E. W.; Novoselov, K. S.; Watanabe, K.; Taniguchi, T.; Geim, A. K.; Blake, P. Hunting for Monolayer Boron Nitride: Optical and Raman Signatures. *Small* **2011**, *7*, 465−468.
(33) Li, H.; Zhang, Q.; Yap, C. C. R.; Tay, B. K.; Edwin, T. H. T.; Olivier, A.; Baillargeat, D. From Bulk to Monolayer MoS_2: Evolution of Raman Scattering. *Adv. Funct. Mater.* **2012**, *22*, 1385−1390.
(34) Lee, C.; Yan, H.; Brus, L. E.; Heinz, T. F.; Hone, J.; Ryu, S. Anomalous Lattice Vibrations of Single- and Few-Layer MoS_2. *ACS Nano* **2010**, *4*, 2695−2700.
(35) Berkdemir, A.; Gutiérrez, H. R.; Botello-Méndez, A. R.; Perea-López, N.; Elías, A. L.; Chia, C.-I.; Wang, B.; Crespi, V. H.; López-Urías, F.; Charlier, J.-C.; Terrones, H.; Terrones, M. Identification of Individual and Few Layers of WS_2 Using Raman Spectroscopy. *Sci. Rep.* **2013**, *3*, 1755.
(36) Lipatov, A.; Lu, H.; Alhabeb, M.; Anasori, B.; Gruverman, A.; Gogotsi, Y.; Sinitskii, A. Elastic Properties of 2D $Ti_3C_2T_x$ MXene Monolayers and Bilayers. *Sci. Adv.* **2018**, *4*, No. eaat0491.
(37) Amarie, S.; Keilmann, F. Broadband-Infrared Assessment of Phonon Resonance in Scattering-Type Near-Field Microscopy. *Phys. Rev. B: Condens. Matter Mater. Phys.* **2011**, *83*, No. 045404.
(38) Patoka, P.; Ulrich, G.; Nguyen, A. E.; Bartels, L.; Dowben, P. A.; Turkowski, V.; Rahman, T. S.; Hermann, P.; Kästner, B.; Hoehl, A.; Ulm, G.; Rühl, E. Nanoscale Plasmonic Phenomena in CVD-Grown MoS_2 Monolayer Revealed by Ultra-Broadband Synchrotron Radiation Based Nano-FTIR Spectroscopy and Near-Field Microscopy. *Opt. Express* **2016**, *24*, 1154−1164.
(39) Kresse, G.; Furthmuller, J. Efficient Iterative Schemes for *ab initio* Total-Energy Calculations Using a Plane-Wave Basis Set. *Phys. Rev. B: Condens. Matter Mater. Phys.* **1996**, *54*, 11169−11186.
(40) Hermann, P.; Hoehl, A.; Patoka, P.; Huth, F.; Rühl, E.; Ulm, G. Near-Field Imaging and Nano-Fourier-Transform Infrared Spectroscopy Using Broadband Synchrotron Radiation. *Opt. Express* **2013**, *21*, 2913−2919.
(41) Hermann, P.; Hoehl, A.; Ulrich, G.; Fleischmann, C.; Hermelink, A.; Kästner, B.; Patoka, P.; Hornemann, A.; Beckhoff, B.; Rühl, E.; Ulm, G. Characterization of Semiconductor Materials Using Synchrotron Radiation-Based Near-Field Infrared Microscopy and Nano-FTIR Spectroscopy. *Opt. Express* **2014**, *22*, 17948−17958.

DOI: 10.1021/acsnano.8b07703
ACS Nano 2018, 12, 12713−12720